NACA RM E51D20

NACA

RESEARCH MEMORANDUM

EXPERIMENTAL INVESTIGATION OF FLOW IN THE ROTATING PASSAGES OF A 48-INCH IMPELLER AT LOW TIP SPEEDS

By Donald J. Michel, Ambrose Ginsburg, and John Mizisin

Lewis Flight Propulsion Laboratory
Cleveland, Ohio

NATIONAL ADVISORY COMMITTEE
FOR AERONAUTICS

WASHINGTON
June 26, 1951

NACA RM E51D20

NATIONAL ADVISORY COMMITTEE FOR AERONAUTICS

RESEARCH MEMORANDUM

EXPERIMENTAL INVESTIGATION OF FLOW IN THE ROTATING PASSAGES OF A 48-INCH IMPELLER AT LOW TIP SPEEDS

By Donald J. Michel, Ambrose Ginsburg, and John Mizisin

SUMMARY

A preliminary study was made of the flow phenomena within the rotating passages of a 48-inch radial-inlet impeller at low tip speeds. Total and static pressures were measured within the impeller passages, at tip speeds of 500 and 700 feet per second, by using a suitable pressure-transfer device to transmit the pressures from the rotating passages to the stationary measuring station.

These studies indicated that the local pressure coefficients were very similar for the two tip speeds. The total-pressure distribution across the passage indicated a region of lower efficiency along the trailing face. The trend in static-pressure distribution agreed with that theoretically determined for straight radial blades. At the maximum weight flow, the large negative angle of attack resulted in flow separation at the driving face and secondary flows, which in turn caused a large loss in total pressure. Little variation was found in pressure from hub to shroud along the blade faces. The power input determined by the integration of pressure difference across the blades agreed closely with the work input obtained from weight-flow and air temperature-rise measurements.

INTRODUCTION

In order to improve the performance of centrifugal compressors, a more complete understanding of the flow phenomena within the rotating impeller passage is necessary. Progress in the improvement of centrifugal compressors has been limited by the scant actual knowledge of the state of the air within the rotating passages; improvements have come largely from successive experimental development.

A preliminary study by the NACA Lewis laboratory was made of the flow within the rotating passages at low tip speeds to determine the state of the air at any point within the impeller. A radial-inlet, radial-discharge centrifugal impeller was instrumented with total-pressure probes and static-pressure taps in the impeller passages. By use of a suitable pressure-transfer device, the state of the air within the impeller was determined at tip speeds of 500 and 700 feet per second over a range of weight flow from choking to surge.

APPARATUS AND INSTRUMENTATION

Test rig. - The experimental research was conducted with an 18-blade, radial-inlet, radial-discharge, 48-inch-diameter centrifugal impeller (fig. 1). A schematic sketch of the compressor installation is shown in figure 2. Ambient room air was drawn through the depression tank into the impeller, discharged into the collector, and then into the single-duct discharge system. The compressor was driven by a 1500-horsepower electric motor through a 1.4 to 1 ratio gear box.

The impeller was similar to that reported in reference 1, with the exception of alterations in the hub-shroud profile necessary for installation of the pressure-transfer devices. The actual blade shape, however, was not changed in the plane normal to the impeller axis. The pertinent blade data are given in table I for a plane normal to the mean height of the blade. The blade cross section is shown in figure 3(a). The blade thickness was corrected to account for the difference in blade area above and below the mean height line, and the correction was of such magnitude as to give approximately equal areas for a truer estimate of the passage area taken up by the blade. The vaneless diffuser was 80 inches in diameter and was designed for a constant area from the impeller tip to the diffuser tip. The clearance between the impeller and the stationary front shroud was 0.070 inch.

Over-all compressor instrumentation. - In the depression tank, five total-pressure probes were installed in a plane before the nozzle at three depths from the wall and four peripheral positions to measure the inlet stagnation pressure. Two 0.030-inch-diameter wall static-pressure taps were installed in the same plane 180° apart to measure the static pressure. The stagnation temperature was measured by two calibrated thermocouple probes designed and built at the Lewis laboratory. These probes were installed in the same instrument plane as the pressure probes, one-third the distance across the tank, and 180° apart.

The same type instrumentation was installed at station 3 in the single discharge duct, 12 diameters from the collector flange as recommended in reference 2.

Static pressure was measured along the stationary front shroud and along the front and rear diffusers at various radii along a diametral line.

Impeller instrumentation. - A schematic diagram of the instrument locations in the impeller passages is shown in figure 3. The total and static pressures were measured at each circled intersection of radius and geometric-streamline. The total-pressure probes were distributed throughout the 18 passages so that any one passage had no more than three probes.

The total-pressure probes were of the Kiel type and were set at the mean height of the blade at any given radius. A calibration of the probes showed a negligible error for a flow-angle range of $\pm 40^{\circ}$, so the probes were set as nearly parallel to the blades as possible.

The static pressure was measured through 0.030-inch-diameter orifices in the impeller hub. In addition to these static measurements, the pressure along both the driving and the trailing blade faces (defined in fig. 3(a)) was measured at the mean height at each radius, and at five equally spaced heights at radii of 14, 18, and $22\frac{1}{2}$ inches as shown in figure 3(a). A static pressure was measured in the center of the passage at the 19-inch radius in alternate passages. Altogether, 148 pressures were measured on the impeller.

Pressure-transfer device. - In order to transfer the pressures from the rotating impeller to the stationary measuring station, a pressure-transfer device was necessary. The device used with the 48-inch compressor was a 21-cell, sealed ball-bearing type; figure 4 shows a sketch of a section of the pressure-transfer device. Each pressure-transfer unit consists of a cavity around the shaft at each pressure-tube outlet; an inner and outer spacer and two sealed ball bearings are used to form this cavity. The pressure is transferred from the rotating shaft through a hole in the inner spacer to the cavity and thence to the stationary outer spacer. The neoprene seals of the bearing prevent leakage from one transfer unit to the next; the rubber seal rings around the inner and outer races of the bearings also prevent leakage around the outer surfaces of the bearings. The whole unit is surrounded by a water jacket, which keeps the bearings cool during operation. Preliminary checks of each transfer unit showed no leakage with vacuums up to 26 inches of mercury in the cavity.

PROCEDURE

The compressor was operated at corrected tip speeds $U/\sqrt{\theta}$ of 500, 700, 782, and 894 feet per second over a range of corrected air weight flow $\frac{W\sqrt{\theta}}{\delta}$ from choking to incipient surge. (All symbols are defined in appendix A.) Only over-all data were taken at the higher tip speeds, whereas complete impeller passage data were taken for several flow rates at 500 and 700 feet per second.

In order to obtain complete data from the 148 pressure measurement stations with the 21-cell pressure-transfer device, it was necessary to use an indexing system. The pressure lines were so arranged that by indexing eight times, complete data could be obtained at a given speed and air weight flow. For each index position, the speed, weight flow, and over-all total-pressure ratio were set so that all three values were as close as possible to previously set points. These points were repeated within an average of ± 1.2 percent for corrected weight flow, ± 0.2 percent for corrected tip speed, and ± 0.6 percent for the over-all total-pressure ratio.

The ambient inlet-air temperature varied from 70° to 90° F. The over-all compressor pressures were measured with mercury and were photographed. The accuracy of the pressures was ± 0.04 inch of mercury.

The pressures in the impeller passages were measured in acetylene tetrabromide and were converted to mercury. The acetylene tetrabromide was calibrated to determine the change in density with temperature of the manometer panel.

The pressures in the passage were measured by balancing them against the pressure in the center of the passage (19-in. radius), which was common to all test runs. This common pressure was then measured, and the actual passage pressure was computed by adding or subtracting the pressure difference. In order to correct for the effect of centrifugal force on the air column in the rotor, the following correction obtained from one-dimensional radial equilibrium and the perfect-gas law was used:

$$(\text{pressure})_c = (\text{pressure})_m \, e^{\frac{2\pi^2 N^2 (r_i^2 - r_{pt}^2)}{gRT_d}}$$

The temperature of the air column, T_d in the exponent, was assumed equal to the disk temperature, which was assumed constant. Upon checking the actual temperature along the rear of the rotor disk from hub to tip, it was found to be almost constant (within $\pm 5^\circ$ F), so an average value was used in the equation. The correction for the centrifugal-force effect varied from 1.6 to 13.2 percent, depending on the impeller speed and the radius of the impeller orifice. A check of the pressure in the center of the passage (19-in. radius) of alternate passages showed little variation in pressure from passage to passage for any given flow condition.

RESULTS AND DISCUSSION

Over-all compressor performance. - The over-all compressor performance at corrected tip speeds of 500, 700, 782, and 894 feet per second are shown in figure 5, plotted in accordance with the recommendations of reference 3. The pressure ratio P_3/P_0 and adiabatic efficiency η_{ad} were based on the measurements made in the discharge duct at station 3. A peak efficiency of 0.72 was obtained at a pressure ratio of 1.65 at a corrected tip speed of 894 feet per second; at 500 feet per second, the peak efficiency was 0.64 at a pressure ratio of 1.18. The efficiency was low because of the large mixing losses which occurred as the flow discharged from the diffuser to the collector outlet pipe.

Static-pressure distribution along blades. - The static-pressure distribution along the driving and trailing faces and the mid-stream line are shown in figures 6 and 7. In figure 6, a comparison of the pressure coefficient ψ along the driving and trailing faces of the impeller blades is shown for 500 and 700 feet per second. The pressure coefficient is defined by the expression

$$\psi = \frac{c_p J T_0 \left[\left(\frac{p}{P_0} \right)^{\frac{\gamma-1}{\gamma}} - 1 \right]}{\frac{U^2}{2g}}$$

The variations of ψ with radius are similar for both values of $U/\sqrt{\theta}$ for the same Q/N value. The plot was checked at other values of Q/N, and the same degree of similarity was noted. Because of this similarity, the flow distribution at only one speed (700 ft/sec) will be discussed. The weight flow rates that will be discussed are those occurring at surge, peak pressure ratio, design angle of attack, and maximum flow.

For the flow rates below maximum, the curves of figure 7 are very similar, showing a gradual rise in static pressure along the radius to the impeller tip. At maximum flow (fig. 7(d)), the large drop in static pressure near the blade entrance on the driving face was probably caused by the large negative angle of attack on the blade, which produces a flow separation at that side of the blade entrance. The static pressure also drops off at the blade tip on the driving face, in order for the blade to unload.

Total-pressure distribution across passage. - The total-pressure distribution across the impeller passage is shown in figure 8. At the lower weight flows (figs. 8(a), (b), and (c)), the pressure distribution uniformly varies across the passage. At the weight flow rate of 30 pounds per second (fig. 8(c)), the total pressure at the driving-face entrance drops off because of the separation of the air from the driving face of the blade, but the distribution in total pressure rapidly achieves a smooth variation across the passage at the larger radii.

The total pressure decreases from the driving face towards the trailing face, which indicates a region of lower efficiency near the trailing face. If the efficiency were 1.00 across the passage, the total pressure would be constant at a given radius. The low-efficiency region at the trailing face is further illustrated in figure 9. The efficiency was determined from the equation developed in appendix B. The efficiency is high on the driving face and reaches a minimum about half-way along the trailing face. The same type of efficiency contour was observed at other flow rates below maximum. The low-energy air (relative to the impeller) appears to move towards the trailing face of the blade. It appears that by some secondary flow process, the exact nature of which is unknown, the low-energy air is replaced on the driving face by higher energy air.

At maximum flow (fig. 8(d)), the large negative angle of attack apparently causes a separation at the driving-face entrance. Here again the variation in total pressure across the passage indicates that the low-energy air moves toward the trailing face and is replaced on the driving face of the blade by higher energy air. The ideal total-pressure ratio is compared with the measured total-pressure ratio near the driving face of the blade (geometric-streamline 1) in figure 10. This comparison is a further indication that the low-energy air is replaced in this plane of measurement by higher energy air, as evidenced by the much greater slope of the actual-pressure-ratio curve than the ideal-pressure-ratio curve from the 13-inch radius to the 18-inch radius.

Static-pressure distribution across passage. - The static-pressure distribution across the impeller passage is shown in figure 11 for each weight flow. In these plots, the pressures at the 12-inch radius were not measured on the blade faces, and at the 13-inch radius, the pressure tap on the wall coincided with the tap at the geometric-streamline 9.

The static-pressure difference between the driving and trailing faces accounts for the torque of the impeller. The trend in pressure distribution across the passage agrees with the theoretically determined distribution for straight blades in reference 4. The trend in the increase in slope of the static-pressure-distribution curves across the passage from inlet to about half-passage length and then the decrease in slope to the tip that was obtained for the theoretical case was also observed for the experimental results.

Pressure distribution from hub to shroud. - Except for the 18-inch radius at the trailing face, there was little change in pressure from hub to shroud along the blade faces, as shown in figure 12. Figure 13 shows the relation between the static pressure along the stationary front shroud and the mean line of the impeller passage at the hub. The agreement between these curves is very good except at the blade entrance, which indicates that the static pressure measured along the stationary shroud is a good indication of the mean pressure in the impeller passage for a radial-inlet impeller.

Power input to impeller. - In order to substantiate further the validity of the pressure data, the power input to the impeller was calculated by two methods.

The first method determined the power from measurements of weight flow and temperature rise through the impeller by the expression

$$HP = Wc_p (T_2 - T_0)$$

The second method determined the power by the integration of the pressure difference across the blade as given by the expression

$$HP = \omega \int \Delta p \; hr \; dr$$

A comparison of the power input obtained by the two methods is shown in figure 14. The agreement is very good up to a weight flow of 30 pounds per second. At the maximum flow of 44 pounds per second, however, the agreement was poor because the power computed by the integration method was very low.

SUMMARY OF RESULTS

An investigation of the flow in the rotating passages of a 48-inch impeller at low tip speeds produced the following results:

1. Local pressure coefficients were very similar for tip speeds of 500 and 700 feet per second.

2. The total-pressure distribution across the passage indicated a region of lower efficiency along the trailing face of the blade.

3. The trend in static-pressure distribution across the impeller passage agreed with that theoretically determined for straight radial blades.

4. At maximum flow, as a result of a large negative angle of attack at the blade entrance, separation at the driving face and secondary flows (the exact nature of which is not known at present) caused large total-pressure losses.

5. There was little variation in pressure from hub to shroud along the blade faces.

6. The static pressure along the stationary front shroud agreed closely with the average pressure in the impeller passage.

7. The power input as determined by weight flow and impeller temperature rise data and by the integration of pressure difference across the blade agreed very closely up to a weight flow of 30 pounds per second.

Lewis Flight Propulsion Laboratory,
National Advisory Committee for Aeronautics,
Cleveland, Ohio.

APPENDIX A

SYMBOLS

The following symbols are used in this report:

c_p	specific heat of air at constant pressure, ft-lb/(lb)($^{\circ}$F)
g	acceleration of gravity, ft/sec^2
HP	power input, hp
ΔH_{ad}	isentropic increase in total enthalpy, ft-lb/lb
ΔH_{act}	actual increase in total enthalpy, ft-lb/lb
h	blade height, ft
J	mechanical equivalent of heat, ft-lb/Btu
N	compressor shaft speed, rps
P	total pressure, in. Hg
p	static pressure, in. Hg
Q	volume flow, cu ft/sec
R	gas constant for air, ft-lb/(lb)($^{\circ}$F)
r	radius, ft
T	total temperature, $^{\circ}$R
U	impeller tip speed, ft/sec
u	tangential component of velocity of air, ft/sec
W	air weight flow, lb/sec
γ	ratio of specific heats for normal air
δ	ratio of actual inlet total pressure to standard sea-level pressure, 29.92 in. Hg

η_{ad} adiabatic efficiency, (reference 2)

θ ratio of actual inlet total temperature to standard sea-level temperature, 518.4° R

ψ pressure coefficient

ω rotor speed, radians/sec

Subscripts:

0 inlet measuring station, (absolute conditions)

2 impeller-outlet measuring station

3 outlet-pipe measuring station, (absolute conditions)

c corrected pressure

d impeller disk

i pressure orifice in impeller, (fig. 3)

m measured pressure

pt pressure orifice in pressure-transfer device, (fig. 4)

r relative conditions

APPENDIX B

DEVELOPMENT OF EXPRESSION FOR IMPELLER EFFICIENCY

$$\eta_{ad} = \frac{\Delta H_{ad}}{\Delta H_{act}} \tag{1}$$

$$\Delta H_{ad} = c_p J T_0 \left[\left(\frac{P_r}{P_0} \right)^{\frac{\gamma-1}{\gamma}} - 1 \right] \tag{2}$$

ΔH_{act} = (total enthalpy relative to blade) - (total absolute enthalpy at inlet)

$$= \left[\frac{\omega r(\omega r+u)}{g} - \frac{(\omega r+u)^2}{2g} + \frac{u^2}{2g} + H_{inlet} \right] - H_{inlet} = \frac{\omega^2 r^2}{2g} \tag{3}$$

$$\eta_{ad} = \frac{2gJc_pT_0 \left[\left(\frac{P_r}{P_0} \right)^{\frac{\gamma-1}{\gamma}} - 1 \right]}{\omega^2 r^2} \tag{4}$$

REFERENCES

1. Johnsen, I. A., Ritter, W. K., and Anderson, R. J.: Performance of a Radial-Inlet Impeller Designed on the Basis of Two-Dimensional-Flow Theory for an Infinite Number of Blades. NACA TN 1214, 1947.

2. NACA Subcommittee on Supercharger Compressors: Standard Procedures for Rating and Testing Centrifugal Compressors. NACA ARR E5F13, 1945.

3. NACA Subcommittee on Compressors: Standard Procedures for Rating and Testing Multistage Axial-Flow Compressors. NACA TN 1138, 1946.

4. Stanitz, John D., and Ellis, Gaylord O.: Two-Dimensional Compressible Flow in Centrifugal Compressors with Straight Blades. NACA Rep. 954, 1950. (Formerly TN 1932.)

TABLE I - BLADE DATA AT MEAN HEIGHT

Radius (in.)	Blade angle (deg)	Total blade height (in.)	Thickness (in.)	
			Actual	Corrected
12.32	57.3	3.30	0.730	0.897
13	55.3	3.05	.714	.873
14	50.9	2.72	.665	.817
16	37.3	2.23	.531	.654
18	20.0	1.91	.445	.545
20	4.0	1.69	.410	.504
21.5	0	1.53	.397	.487
22.5	0	1.45	.389	.478
23.5	4.4	1.40	.380	.467

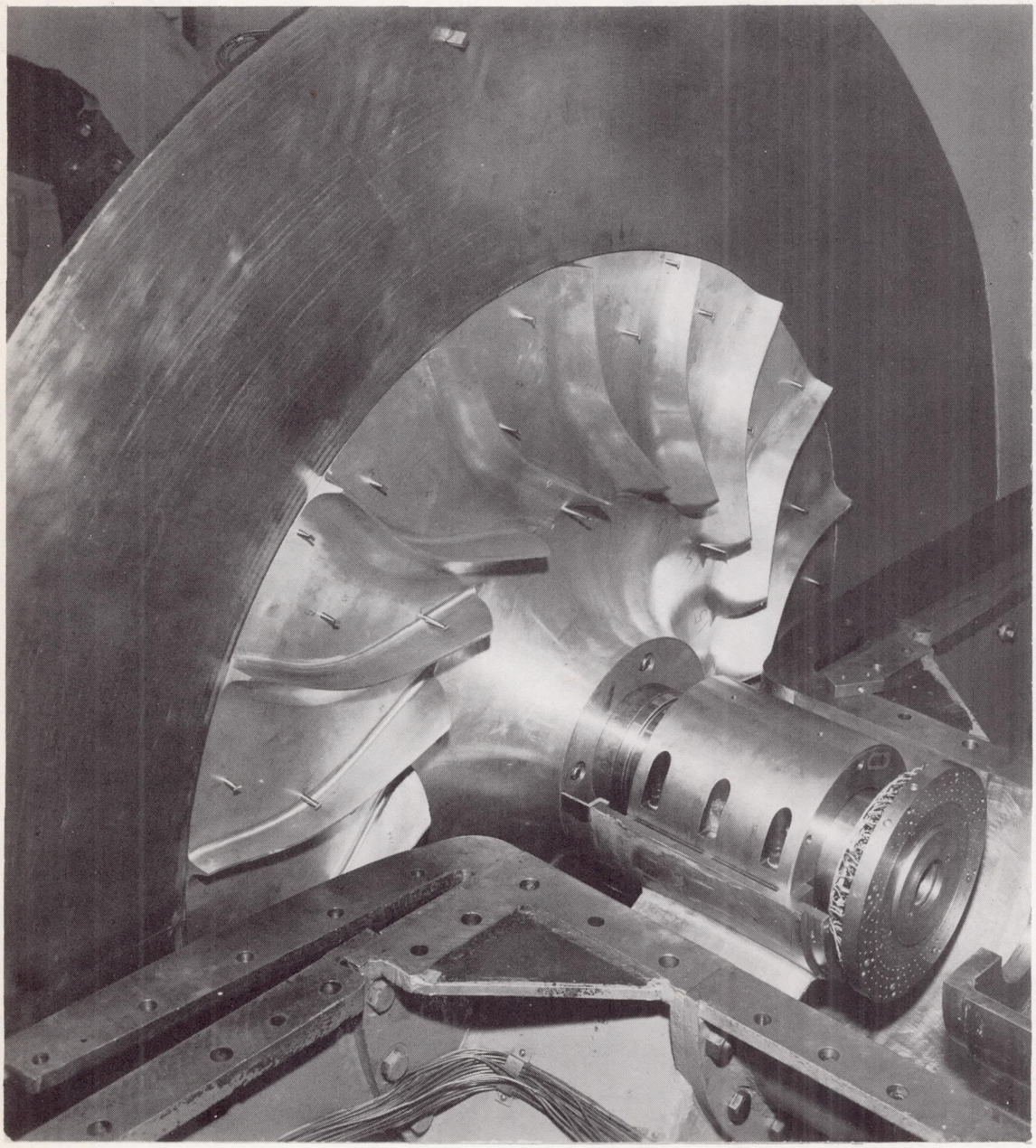

NACA
C-25106

Figure 1. - Radial-inlet impeller used in experimental investigation of flow within rotating passages.

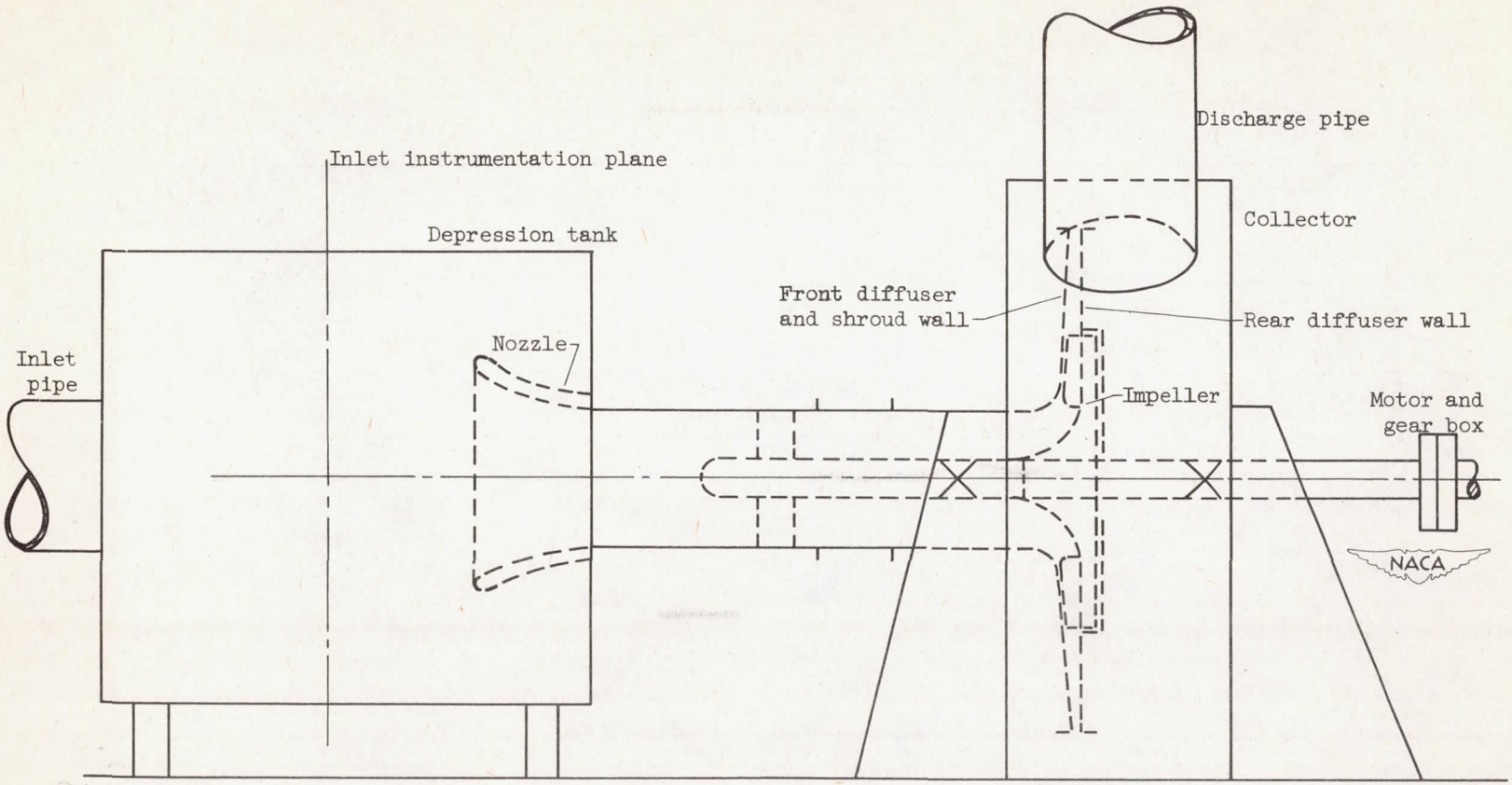

Figure 2. - Schematic diagram of 48-inch-compressor installation.

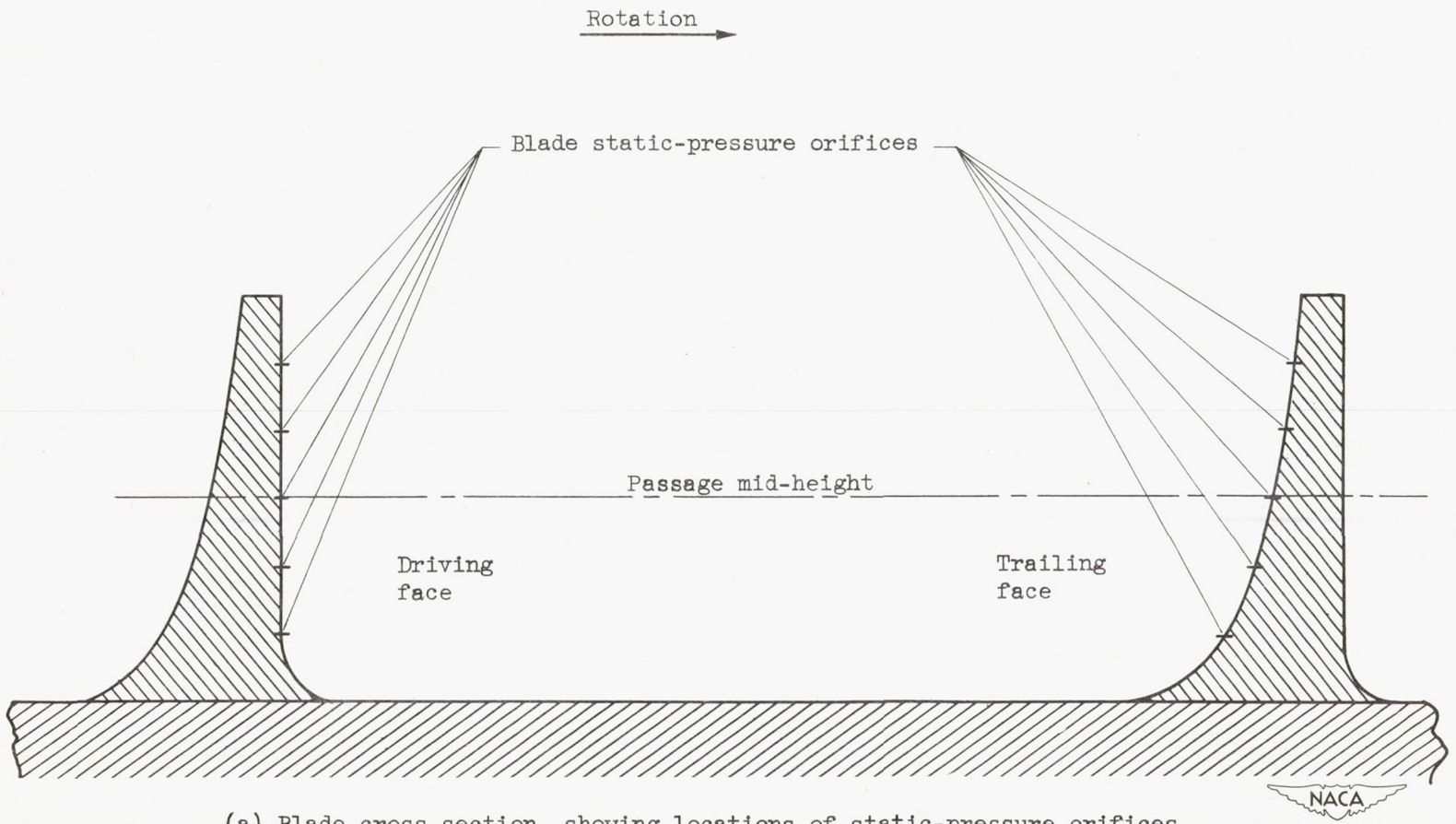

(a) Blade cross section, showing locations of static-pressure orifices.

Figure 3. - Instrumentation for investigation of flow within rotating passages.

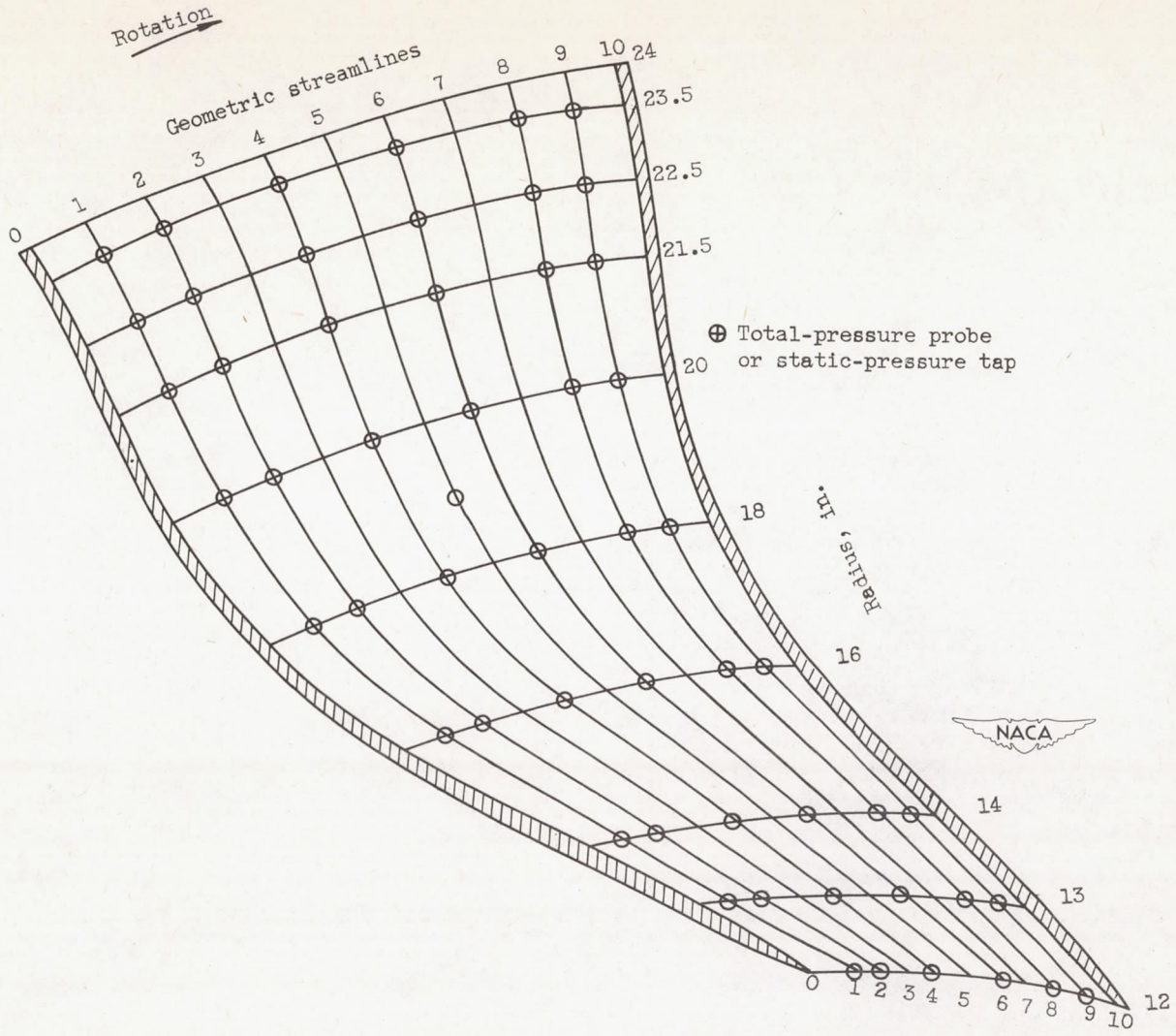

(b) Schematic layout of instrumentation in impeller passage (blade thickness at shroud).

Figure 3. - Concluded. Instrumentation for investigation of flow within rotating passages.

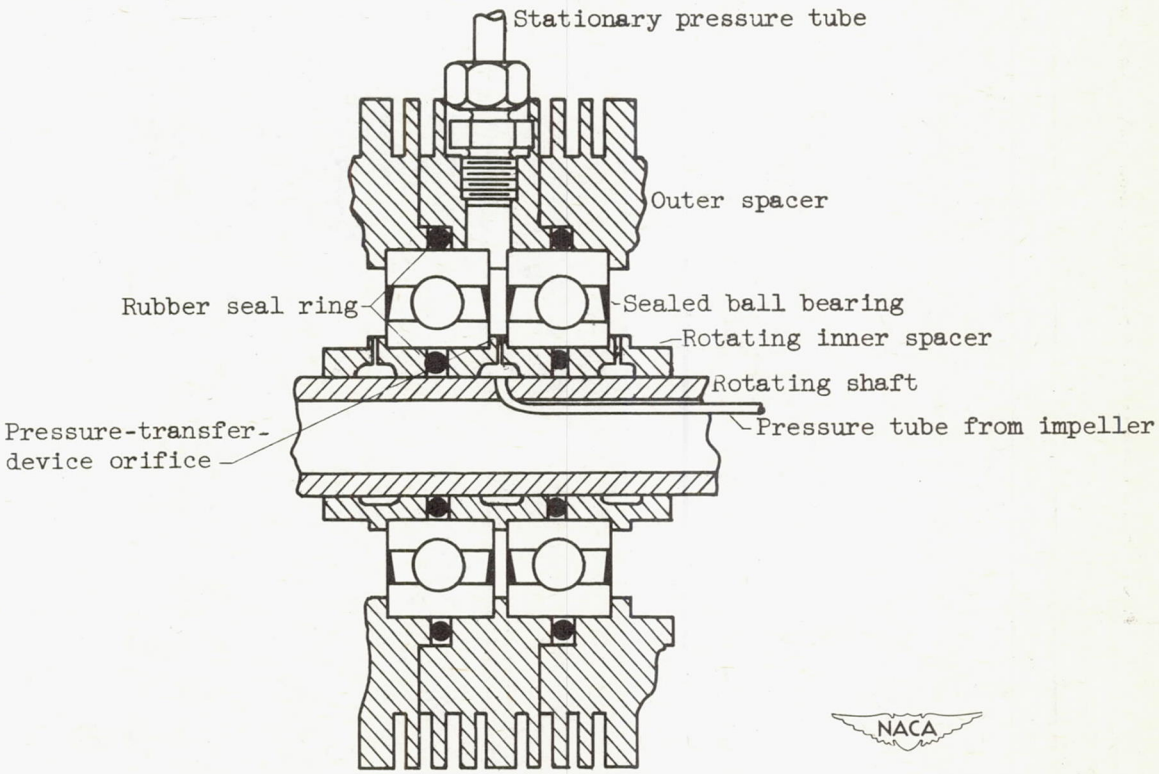

Figure 4. - Section of pressure-transfer device.

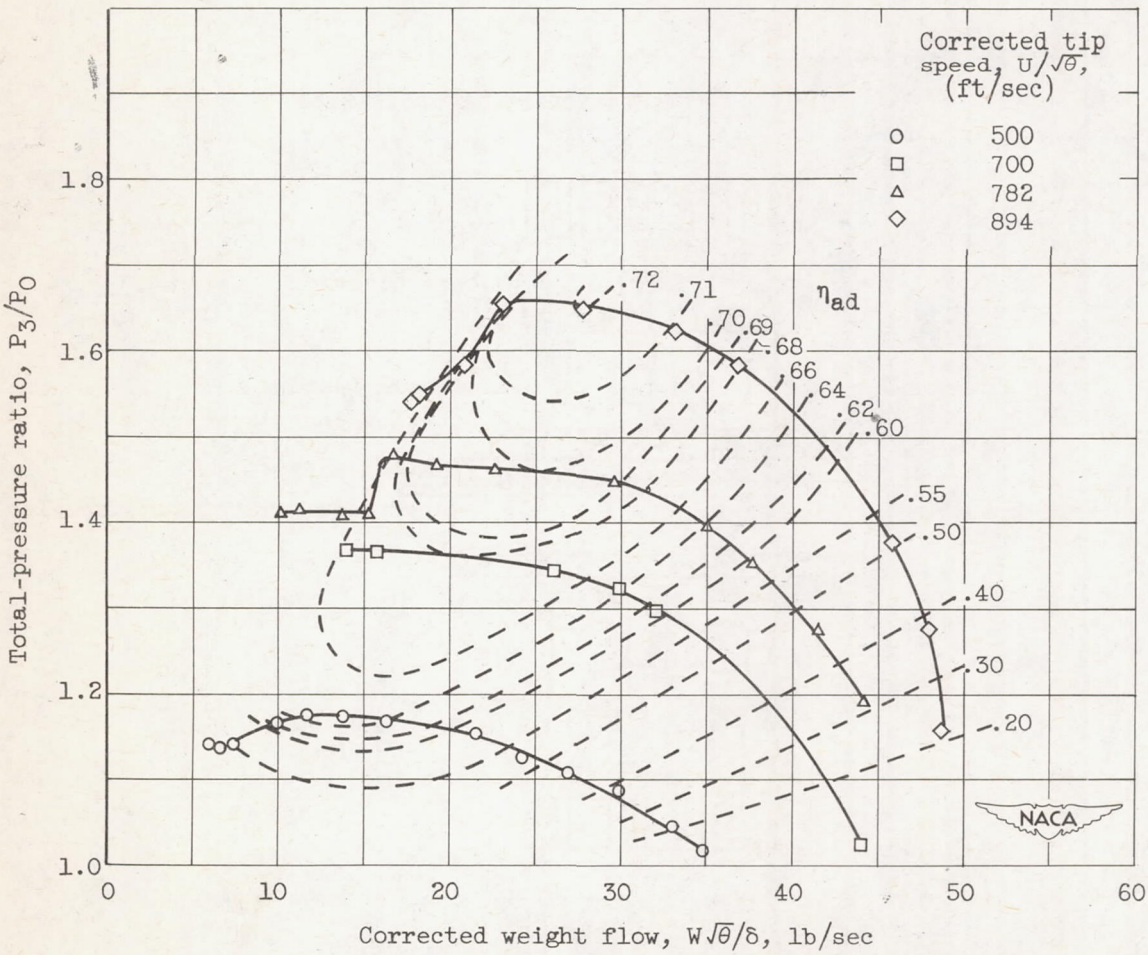

Figure 5. - Over-all performance of impeller and vaneless diffuser.

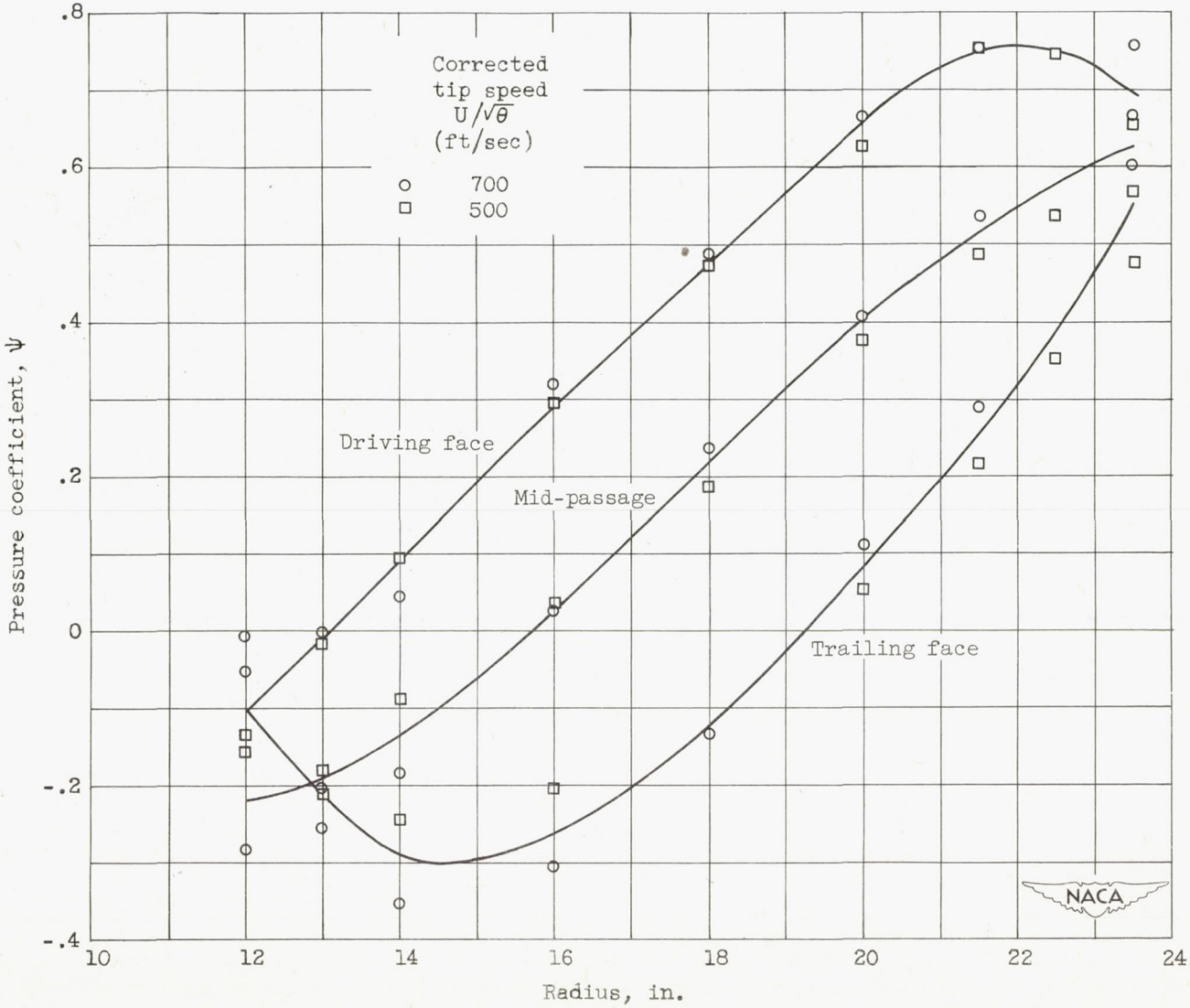

Figure 6. - Pressure distribution along blade faces at same load coefficient.

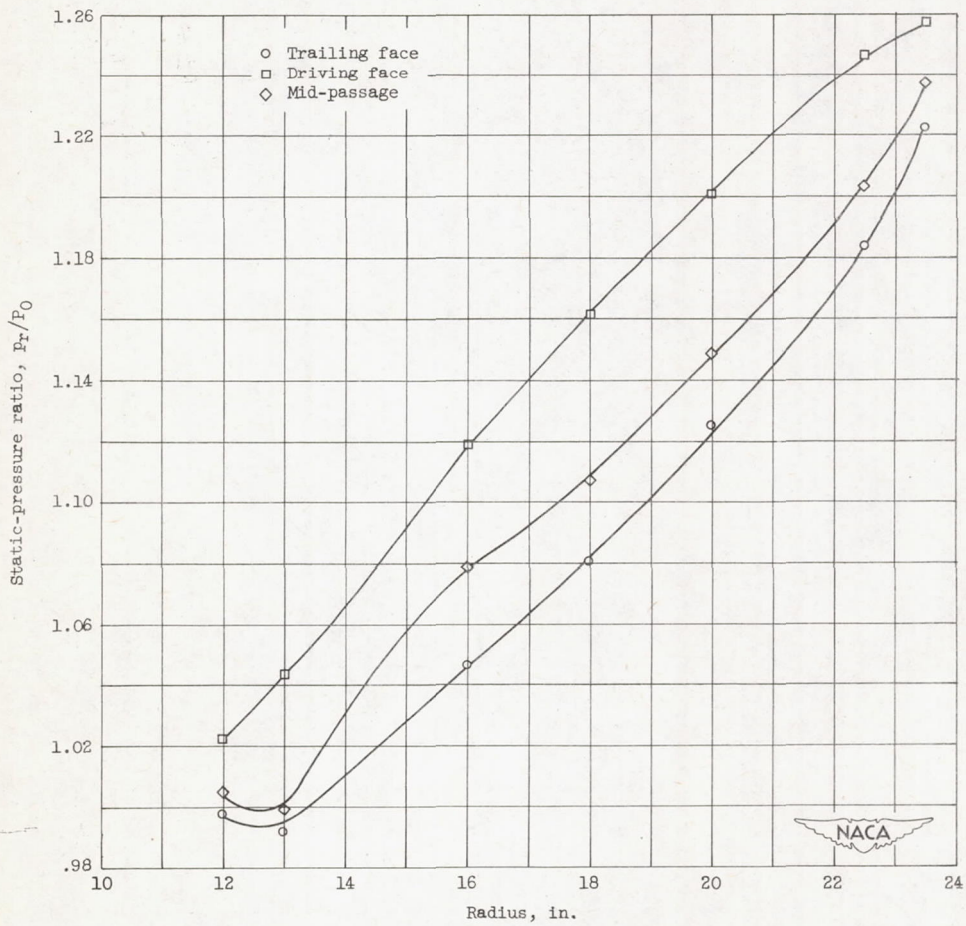

(a) $W\sqrt{\theta}/\delta$ = 14 pounds per second; $U/\sqrt{\theta}$ = 700 feet per second.

Figure 7. - Static-pressure distribution along blade faces and mid-passage.

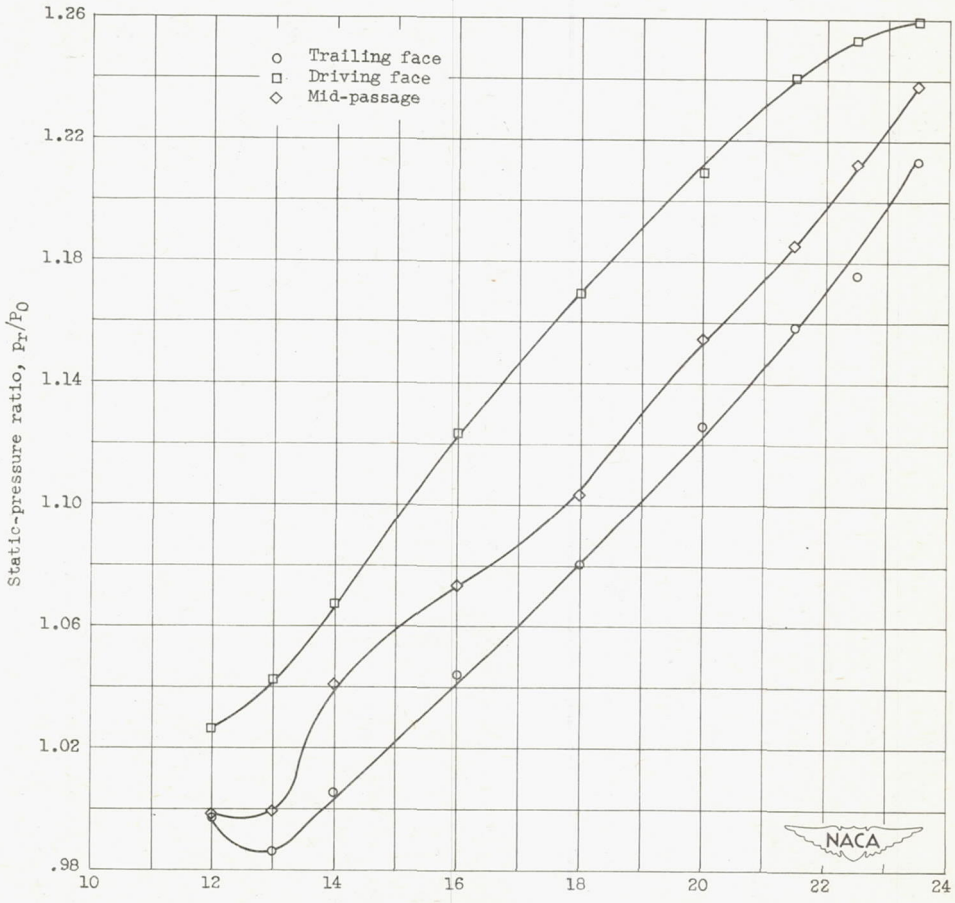

(b) $W\sqrt{\theta}/\delta$ = 15.9 pounds per second; $U/\sqrt{\theta}$ = 700 feet per second.

Figure 7. - Continued. Static-pressure distribution along blade faces and mid-passage.

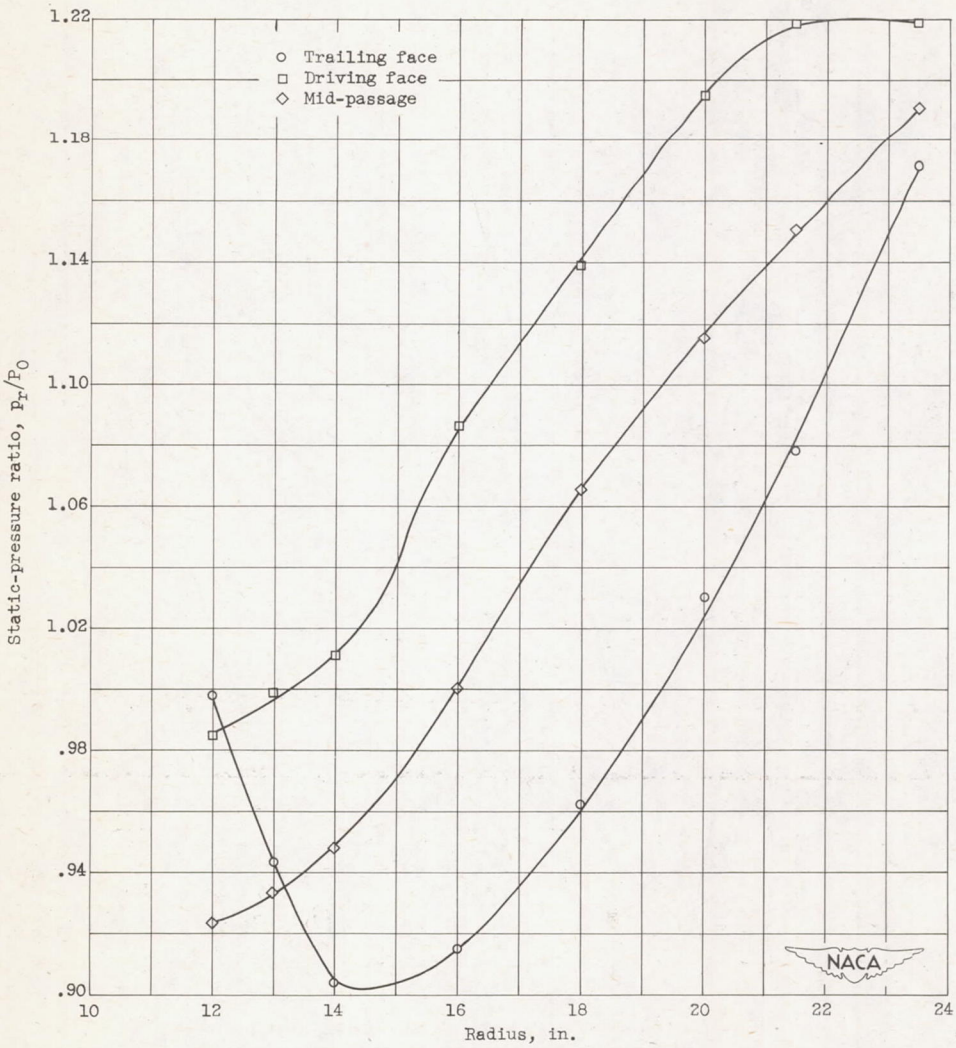

(c) $W\sqrt{\theta}/\delta$ = 30 pounds per second; $U/\sqrt{\theta}$ = 700 feet per second.

Figure 7. - Continued. Static-pressure distribution along blade faces and mid-passage.

(d) $W\sqrt{\theta}/\delta$ = 44 pounds per second; $U/\sqrt{\theta}$ = 700 feet per second.

Figure 7. - Concluded. Static-pressure distribution along blade faces and mid-passage.

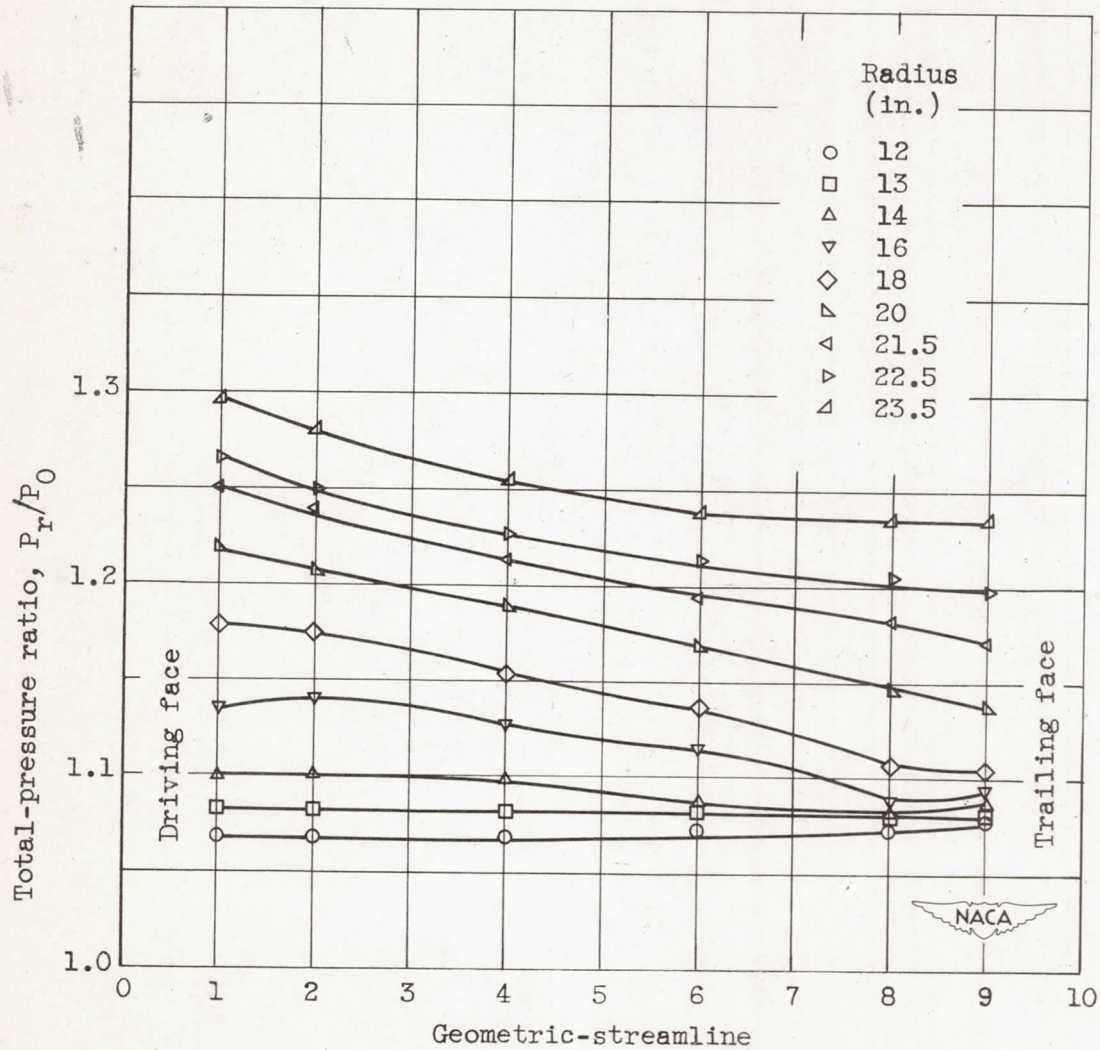

(a) $W\sqrt{\theta}/\delta$ = 14 pounds per second; $U/\sqrt{\theta}$ = 700 feet per second.

Figure 8. - Total-pressure distribution across impeller passage at several radii.

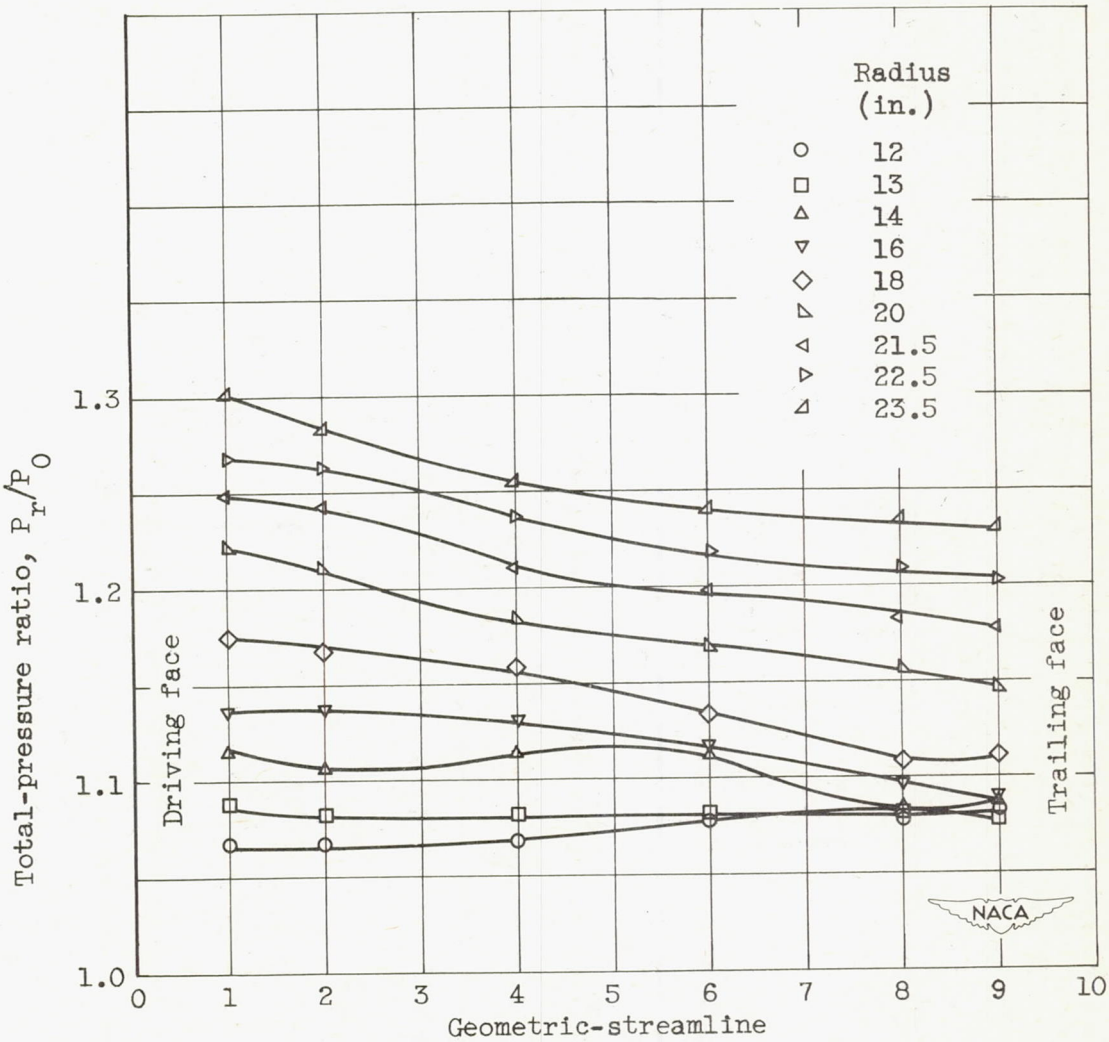

(b) $W\sqrt{\theta}/\delta$ = 15.9 pounds per second; $U/\sqrt{\theta}$ = 700 feet per second.

Figure 8. - Continued. Total-pressure distribution across impeller passage at several radii.

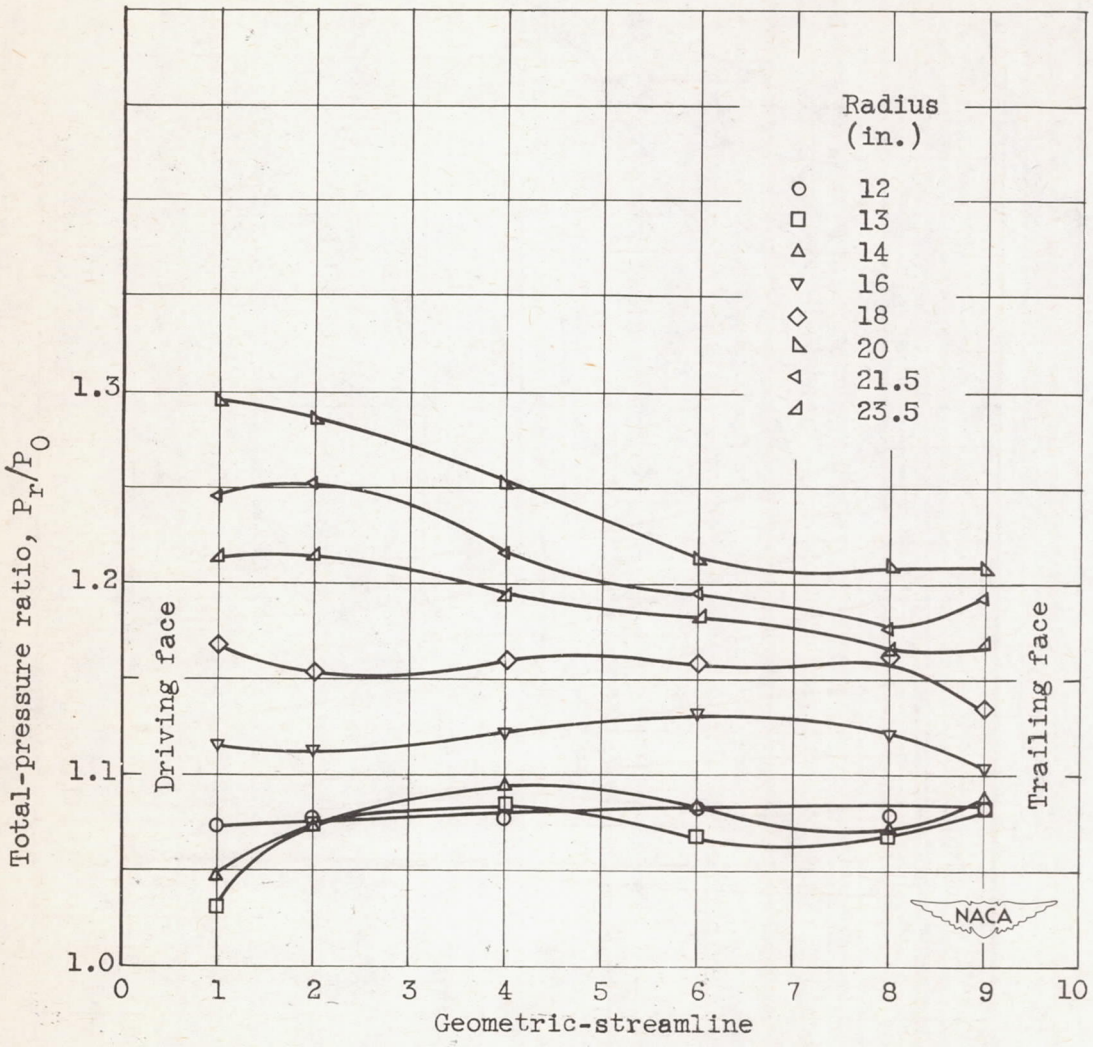

(c) $W\sqrt{\theta}/\delta$ = 30 pounds per second; $U/\sqrt{\theta}$ = 700 feet per second.

Figure 8. - Continued. Total-pressure distribution across impeller passage at several radii.

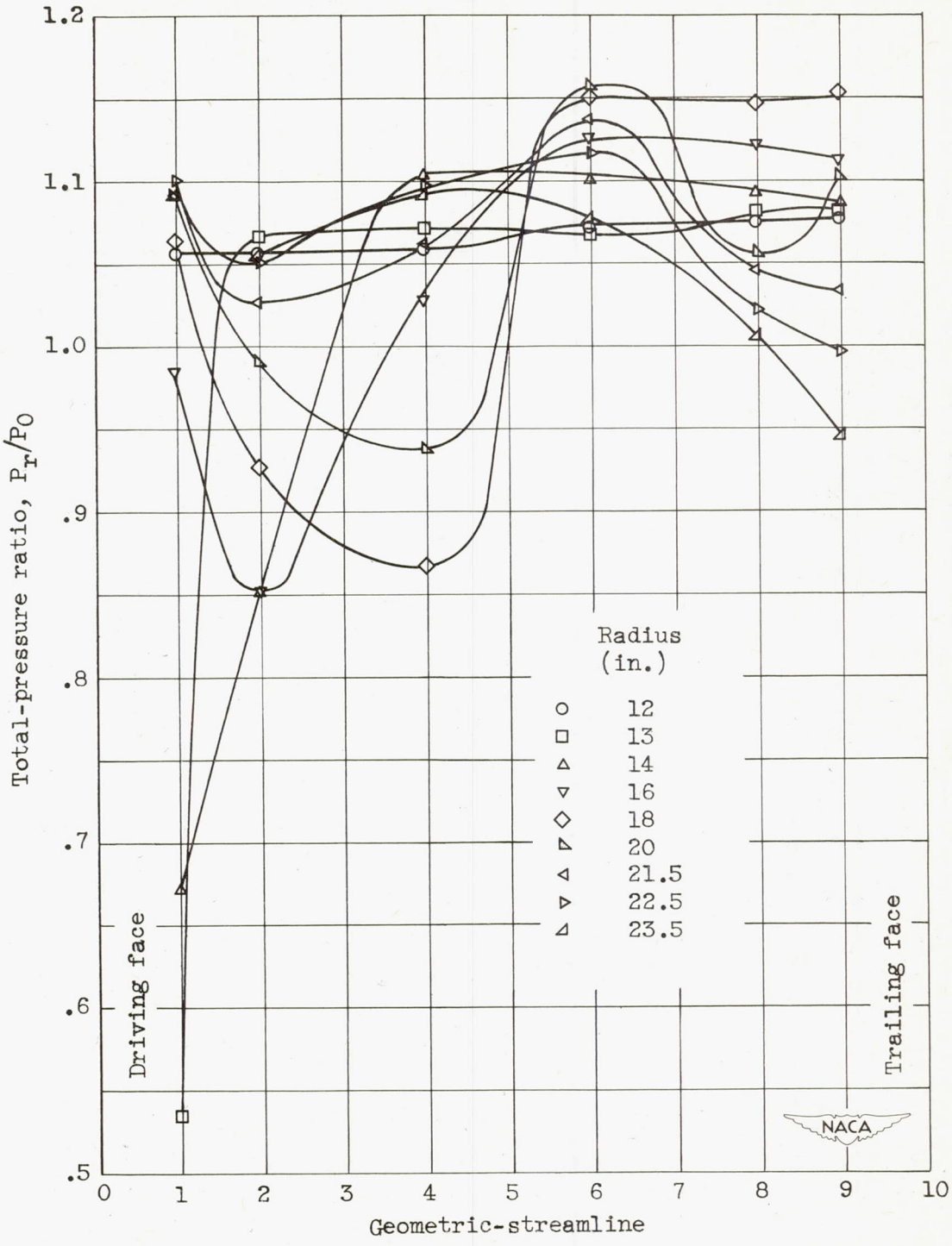

(d) $W\sqrt{\theta}/\delta$ = 44 pounds per second; $U/\sqrt{\theta}$ = 700 feet per second.

Figure 8. - Concluded. Total-pressure distribution across impeller passage at several radii.

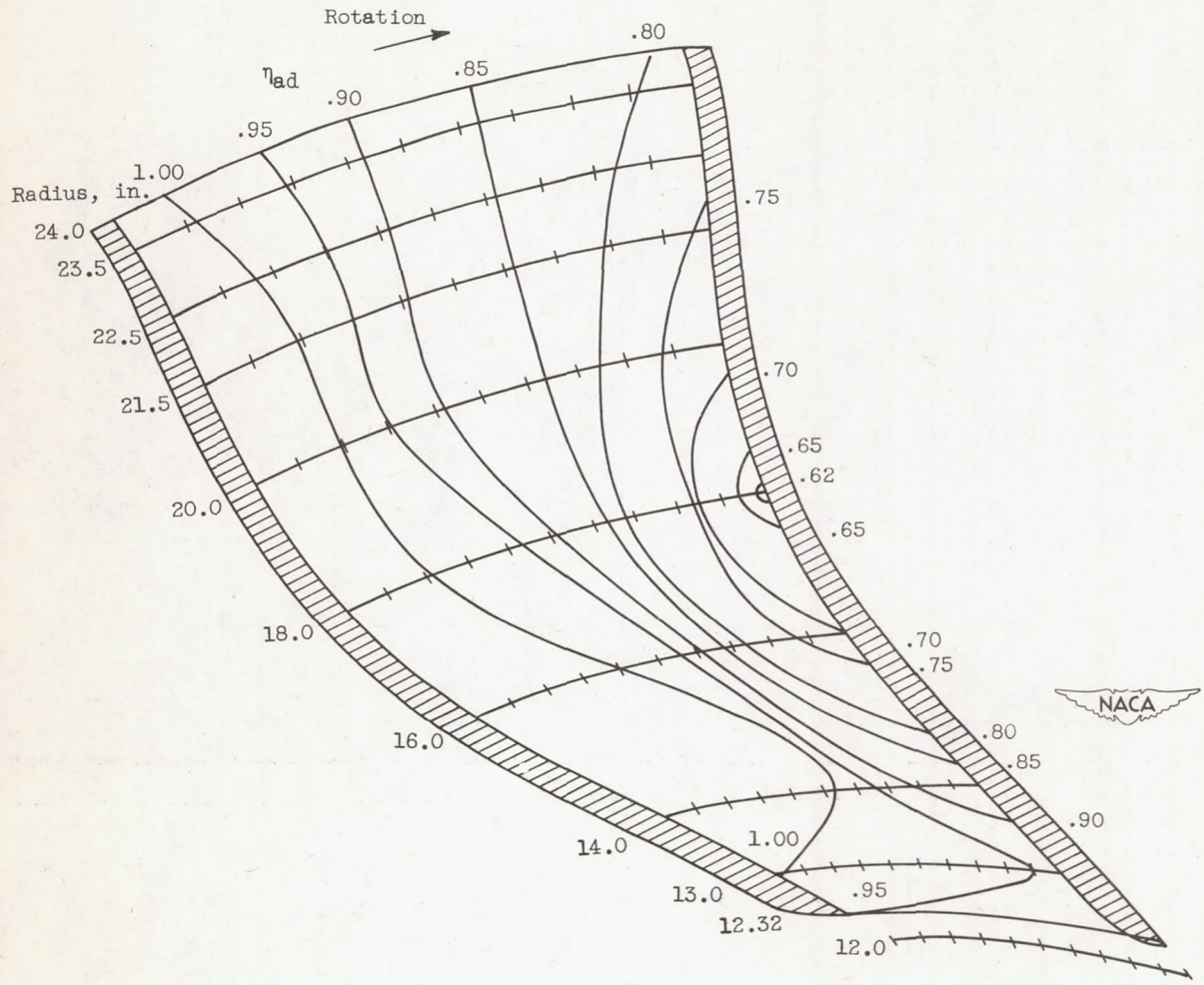

Figure 9. - Efficiency contour through passage at $W\sqrt{\theta}/\delta$ = 15.9 pounds per second and $U/\sqrt{\theta}$ = 700 feet per second.

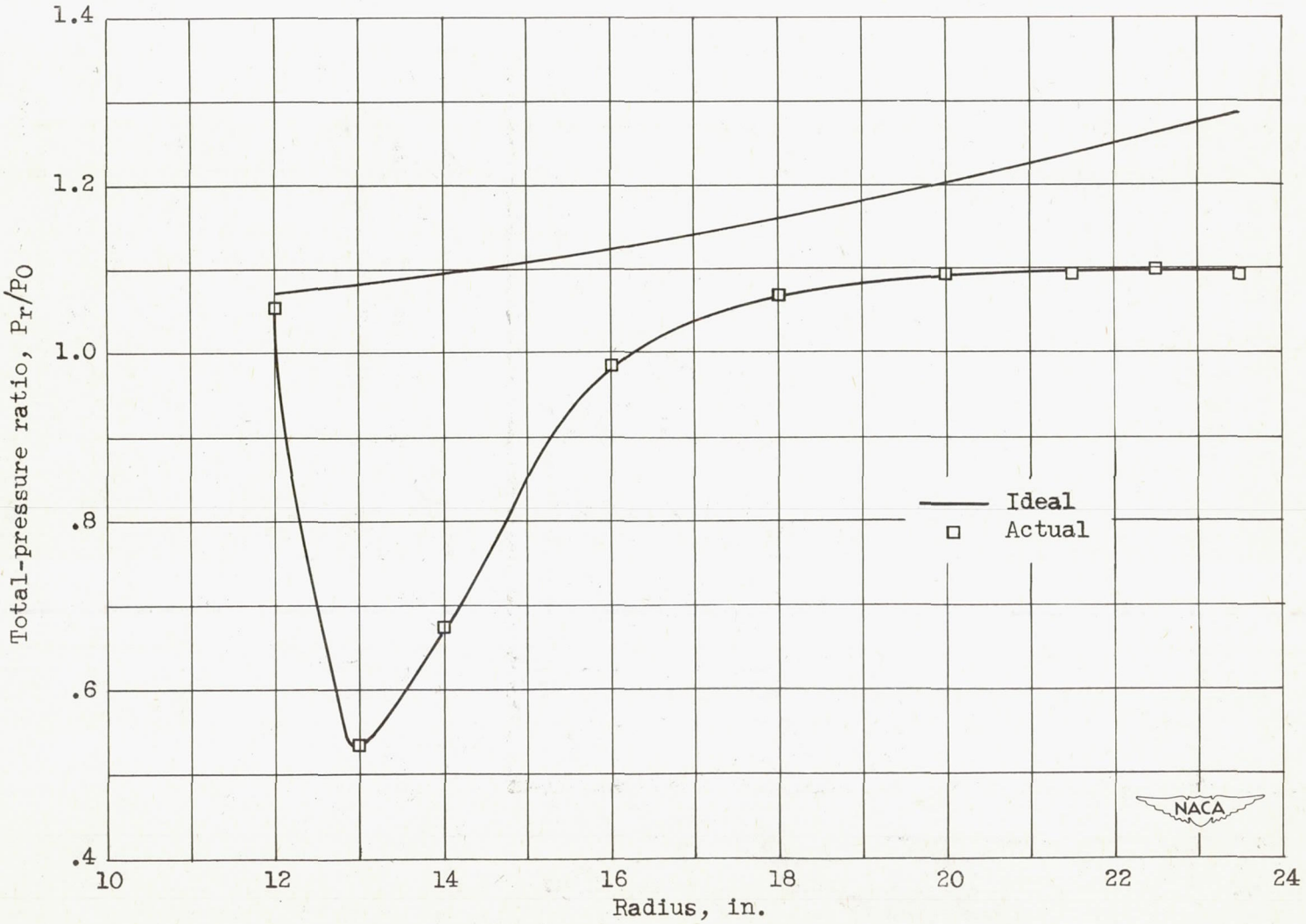

Figure 10. - Ideal and actual total-pressure ratio along driving face at $W\sqrt{\theta}/\delta$ = 44 pounds per second and $U/\sqrt{\theta}$ = 700 feet per second.

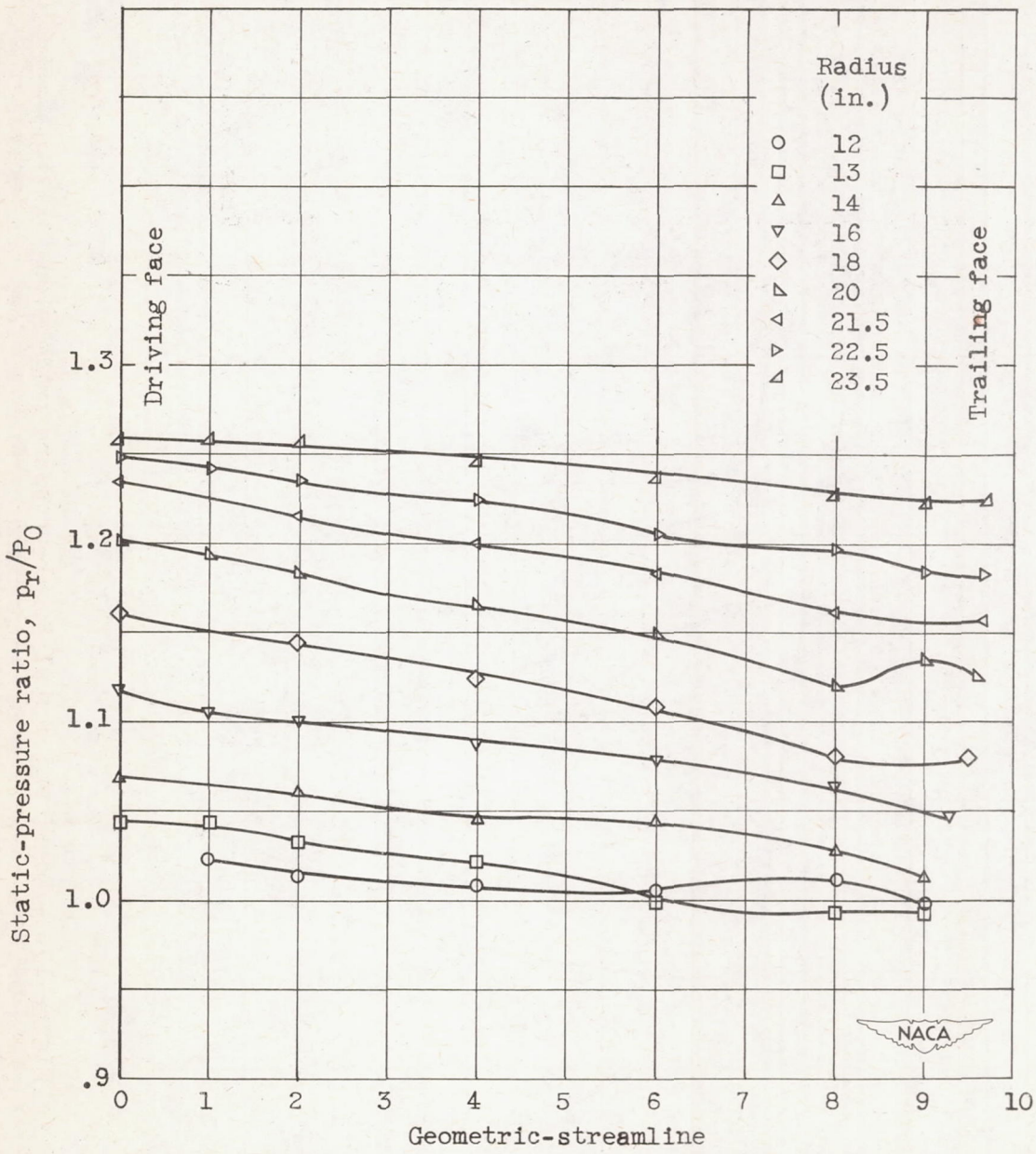

(a) $W\sqrt{\theta}/\delta$ = 14 pounds per second; $U/\sqrt{\theta}$ = 700 feet per second.

Figure 11. - Static-pressure distribution across impeller passage at several radii.

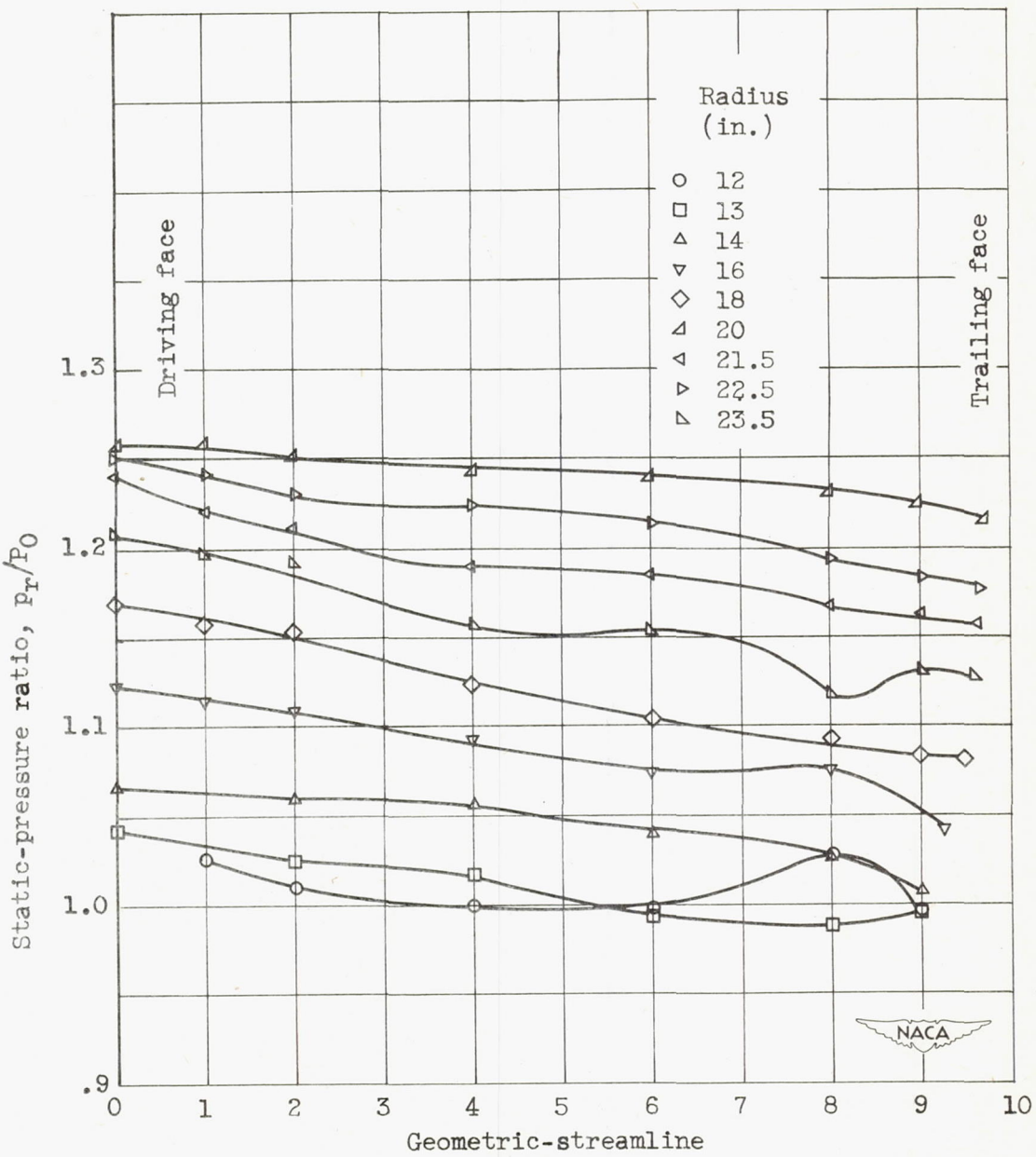

(b) $W\sqrt{\theta}/\delta$ = 15.9 pounds per second; $U/\sqrt{\theta}$ = 700 feet per second.

Figure 11. - Continued. Static-pressure distribution across impeller passage at several radii.

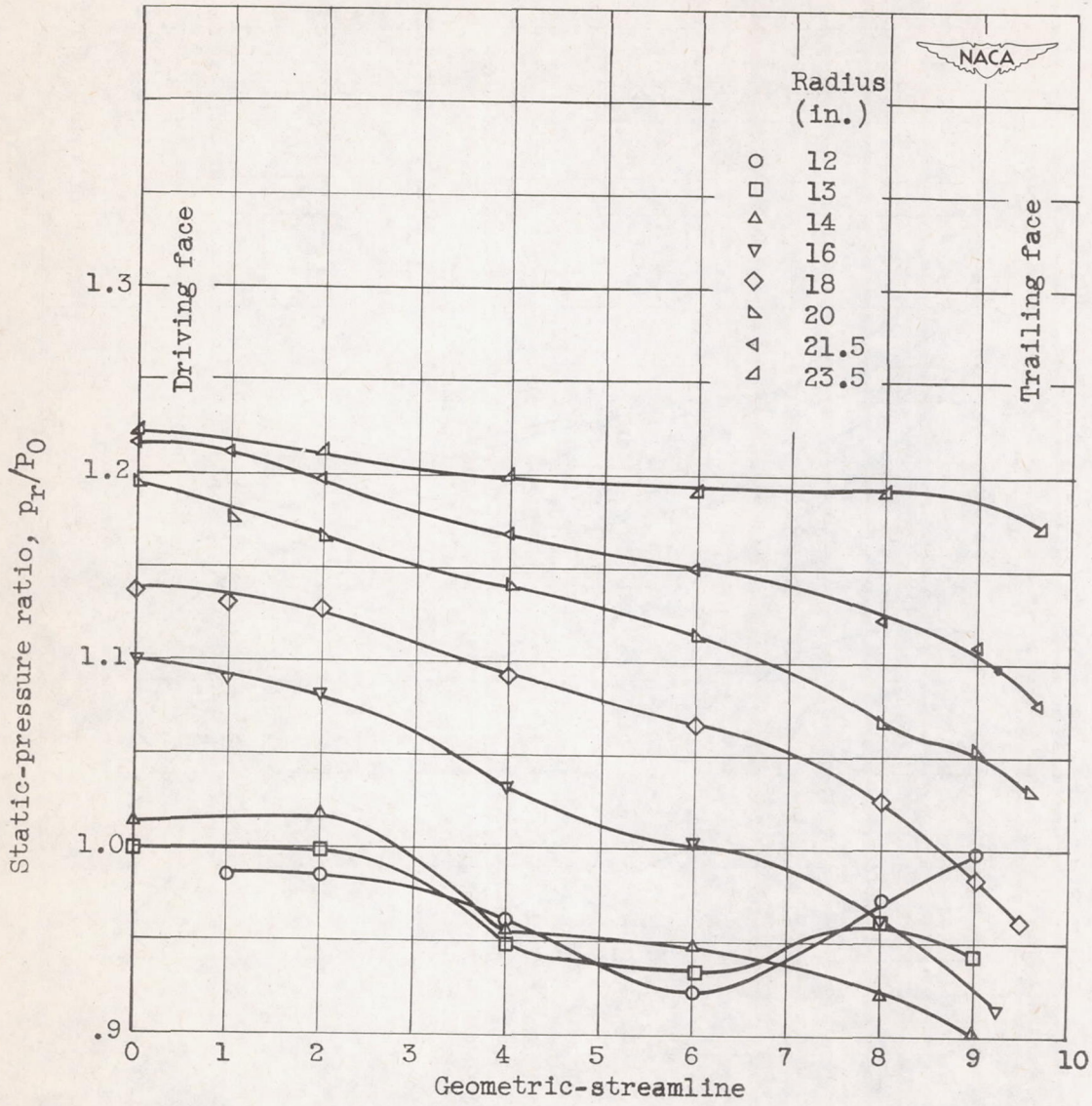

(c) $W\sqrt{\theta}/\delta$ = 30 pounds per second; $U/\sqrt{\theta}$ = 700 feet per second.

Figure 11. - Continued. Static-pressure distribution across impeller passage at several radii.

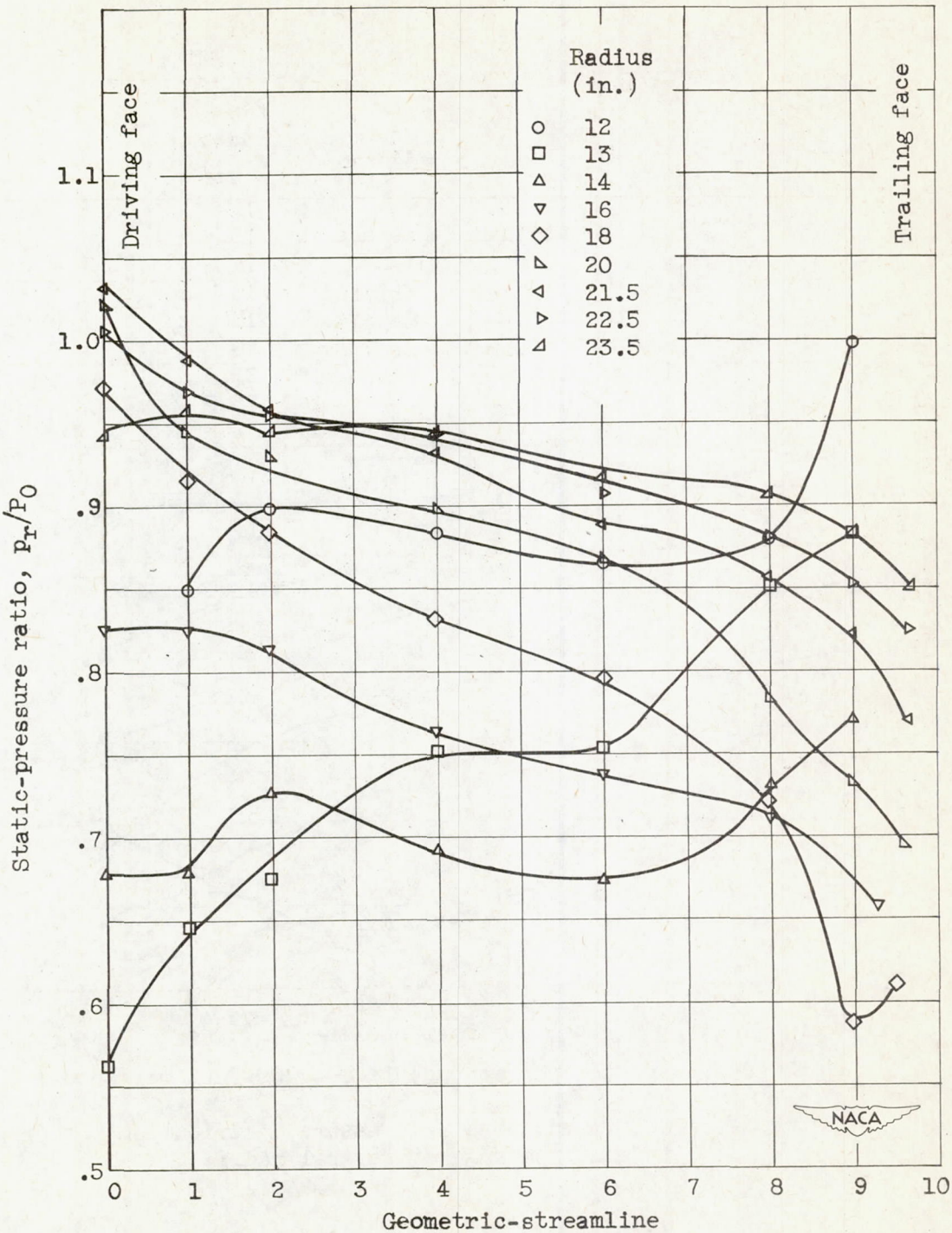

(d) $W\sqrt{\theta}/\delta$ = 44 pounds per second; $U/\sqrt{\theta}$ = 700 feet per second.

Figure 11. - Concluded. Static-pressure distribution across impeller passage at several radii.

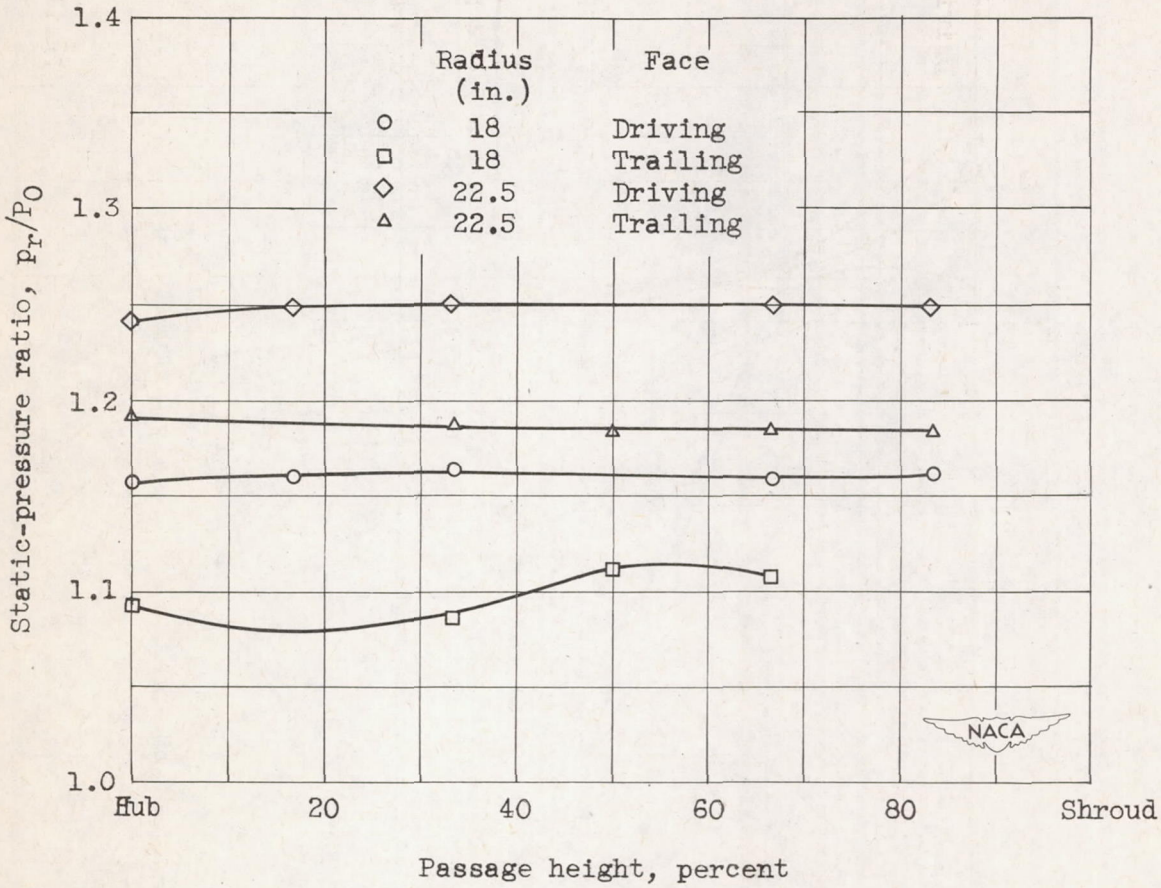

Figure 12. - Static-pressure variation from hub to shroud at $W\sqrt{\theta}/\delta$ = 15.9 pounds per second and $U/\sqrt{\theta}$ = 700 feet per second.

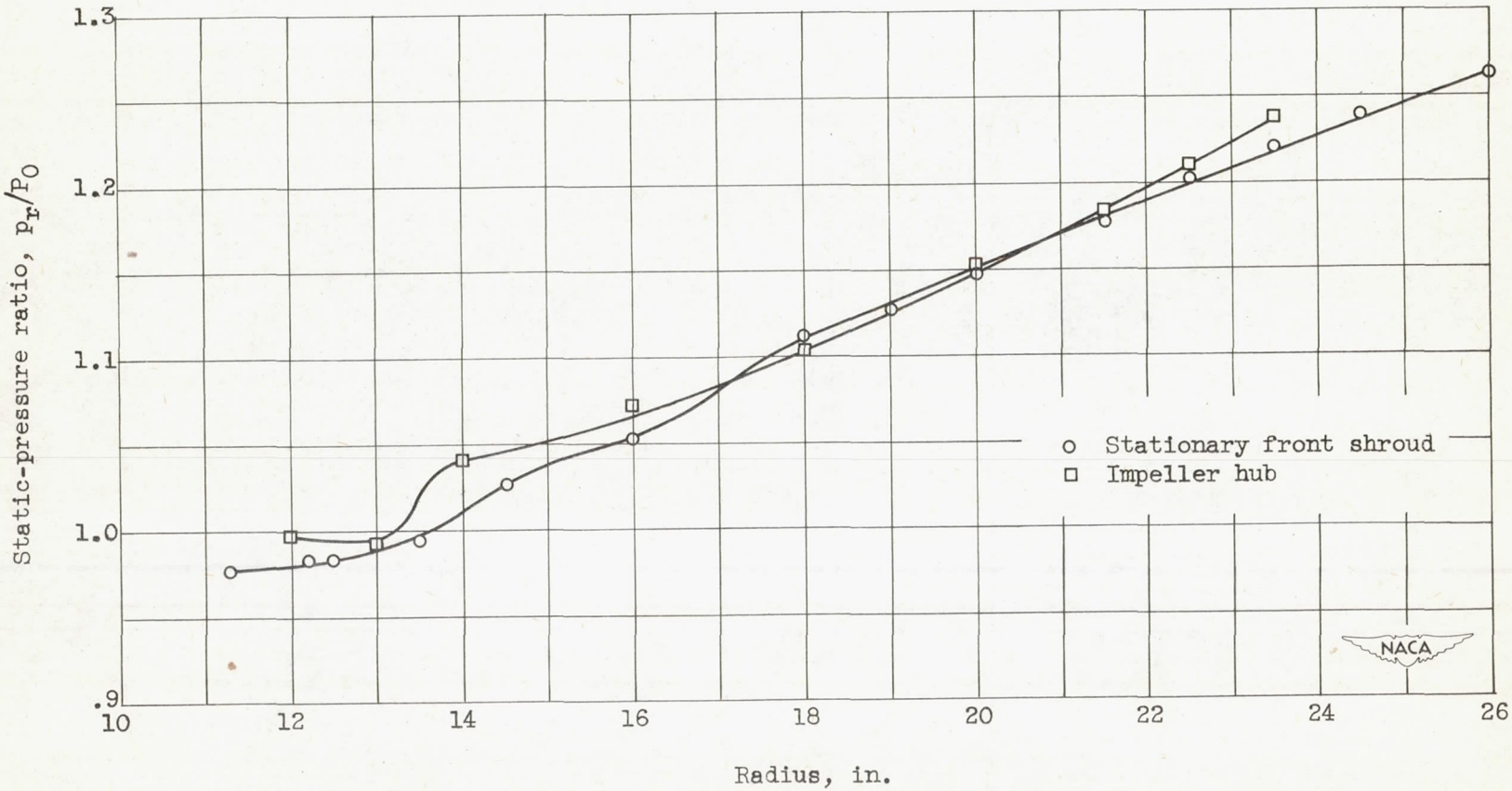

Figure 13. - Comparison of static-pressure ratio along impeller hub and stationary front shroud at $W\sqrt{\theta}/\delta$ = 15.9 pounds per second and $U/\sqrt{\theta}$ = 700 feet per second.

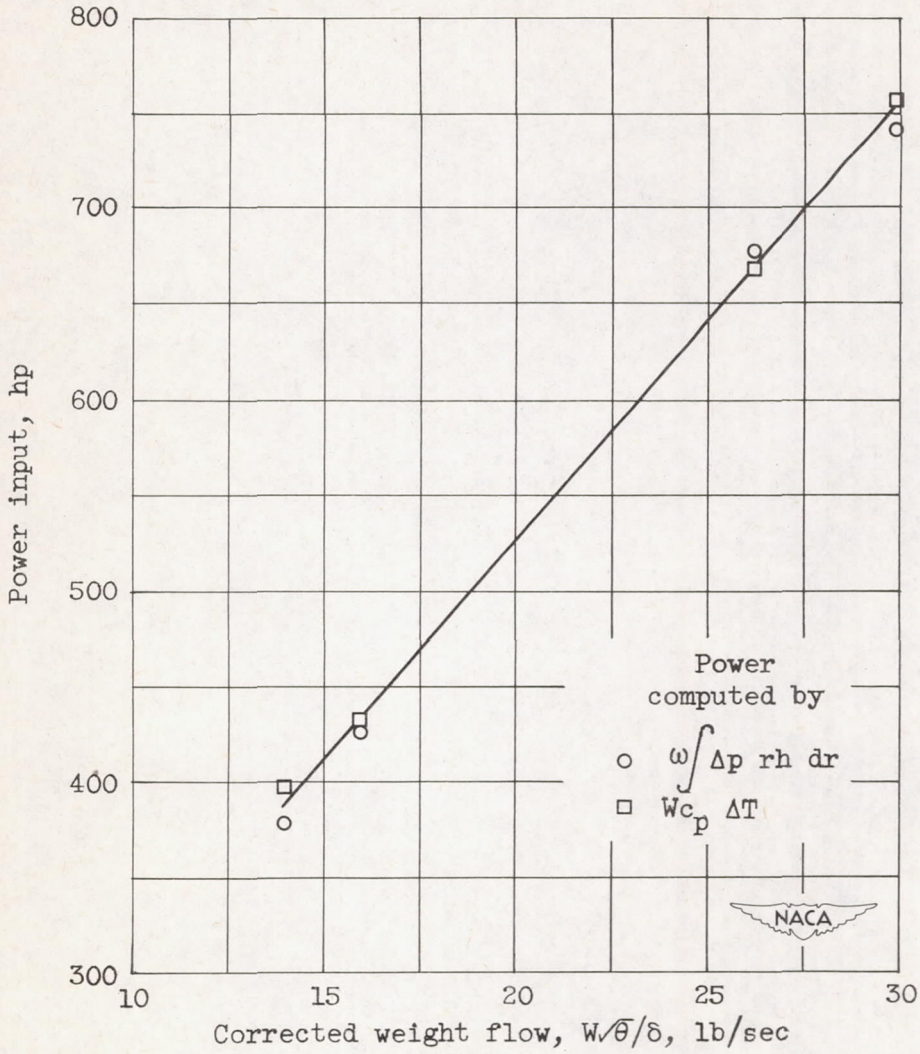

Figure 14. - Power input to impeller based on integrated pressure drop along blades and on measurements.